Nanoscale Res Lett (2010) 5:1137–1143
DOI 10.1007/s11671-010-9616-z

NANO EXPRESS

Fabrication of vertically aligned Pd nanowire array in AAO template by electrodeposition using neutral electrolyte

Nevin Taşaltın · Sadullah Öztürk · Necmettin Kılınç · Hayrettin Yüzer · Zafer Ziya Öztürk

Received: 17 December 2009 / Accepted: 16 April 2010 / Published online: 1 May 2010
© The Author(s) 2010. This article is published with open access at Springerlink.com

Abstract A vertically aligned Pd nanowire array was successfully fabricated on an Au/Ti substrate using an anodic aluminum oxide (AAO) template by a direct voltage electrodeposition method at room temperature using diluted neutral electrolyte. The fabrication of Pd nanowires was controlled by analyzing the current–time transient during electrodeposition using potentiostat. The AAO template and the Pd nanowires were characterized by scanning electron microscopy (SEM), energy-dispersive X-ray (EDX) methods and X-Ray diffraction (XRD). It was observed that the Pd nanowire array was standing freely on an Au-coated Ti substrate after removing the AAO template in a relatively large area of about 5 cm^2, approximately 50 nm in diameter and 2.5 μm in length with a high aspect ratio. The nucleation rate and the number of atoms in the critical nucleus were determined from the analysis of current transients. Pd nuclei density was calculated as 3.55×10^8 cm^{-2}. Usage of diluted neutral electrolyte enables slower growing of Pd nanowires owing to increase in the electrodeposition potential and thus obtained Pd nanowires have higher crystallinity with lower dislocations. In fact, this high crystallinity of Pd nanowires provides them positive effect for sensor performances especially.

Keywords Palladium · Pd nanowires · AAO template · Electrodeposition · Nucleation · Nanomaterials

N. Taşaltın · S. Öztürk · N. Kılınç · Z. Z. Öztürk (✉)
Department of Physics, Gebze Institute of Technology, Cayirova Campus, PO Box 141, 41400 Gebze-Kocaeli, Turkey
e-mail: zozturk@gyte.edu.tr

H. Yüzer · Z. Z. Öztürk
TÜBİTAK-Marmara Research Center, P.K.21, 41470 Gebze-Kocaeli, Turkey

Introduction

Metal nanowires are expected to play a major role in future nanotechnologies. Surface effect, small-size effect and even quantum effects are thus caused and severely affect the physical and chemical properties of these nanomaterials that differ significantly from their bulk counterparts. Such unusual properties have generated interest in nanomaterials for potential applications in electronics, optics, magnetism, sensors, energy storage and catalysis [1–3]. Controllable growth of metallic nanowires has been a topic of continuing investigation, because of the need to obtain high-performance high-density nanoelectronic devices such as field-effect transistors (FETs), chemical and biological sensors [4–7]. In order to prepare the metal nanowire arrays, it has been considered that the electrodeposition of the metal nanowires into a template is the simplest and most versatile approach since it does not utilize expensive and sophisticated lithographic processes for defining nanomaterials [8–10]. The template method has been accomplished using a variety of templates, which are polycarbonate membranes, nanochannel alumina and anodized aluminum oxides (AAO). AAO template especially is an ideal template to the synthesis of metal nanowires as it has good mechanical strength and thermal stability with good controllability of nanowire dimensions [11–13].

To date, palladium is the most preferred active material for catalytic combustion, methanol oxidation, hydrogen sensors and hydrogen storage devices due to its high selectivity and affinity to hydrogen. Hydrogen is adsorbed and dissociated spontaneously in palladium and its alloys [14, 15]. Therefore, Pd is a very special metal, but only a limited number of reports describe the fabrication of Pd nanowires [16–21]. Favier et al. [16] decorated the edge

steps on a graphite surface with Pd by electrodeposition using an electrolyte containing 2 mM Pd^{4+} ions (in 0.1 M HCl or $HClO_4$) and then obtained horizontal Pd nanowires. Then, Kim et al. [17] prepared Pd nanowire arrays with an aspect ratio of 10 using Si-based AAO template by pulsed-current electrodeposition and utilizing a commercial electrolyte [18]. Kartopu et al. [19] synthesized Pd nanowires on Au sheet with AAO template using acidic electrolyte and applying constant voltage. Recently, Cheng et al. [20] prepared Pd nanowires on Ti substrate using AAO template by pulse electrodeposition for studying the electrocatalytic activity of Pd nanowires. Cherevko et al. [21] fabricated conoidal palladium nanowire and nanotube arrays by electrochemical deposition into the branched pores of an alumina template.

Mechanism of thin-film metal deposition and structures of electrodeposits on metal substrates have been extensively studied using various electrochemical methods [22–24]. Despite the technological importance, the mechanism of electrodeposition on a metallic substrate of metallic nanowires has not attracted much attention. Moreover, nucleation and growth of Pd nanowire array on a metal electrode by electrochemical deposition have not been studied yet in detail. More studies are needed to understand the complex nature and mechanism of the electrodeposition of the Pd nanowires on metal electrodes. Keeping such potential applications, a few studies on the nucleation and growth of metallic particles through electrodeposition processes were carried out during past decades. In this paper, we focused on the fabrication of vertical Pd nanowire arrays in AAO template/Au/Ti structure by direct voltage electrodeposition. The fabrication process is similar to the study by Kartopu and his coworkers, but our electrolyte's pH is neutral (7) and has fewer components. We reported new impressive results on the mechanism and kinetics of the initial stages of Pd electrodeposition in AAO template, nucleation and growth kinetics of Pd nanowires endowed with high crystallinity.

Experimental

Anodic aluminum oxide templates were fabricated through a two-step anodization of high-purity aluminum foils [25, 26]. The obtained AAO templates are prepared for Pd nanowire using electrodeposition method as follows: A thin gold film was evaporated onto one surface of the AAO as-prepared template that serves as the working electrode attached with silver epoxy to Ti foil as substrate. The used Ti foil was polished and cleaned before. Then, the remaining aluminum of the AAO template, which was the opposite side of the Au film, was etched in 5 wt% $HgCl_2$ for complete removing. After that, the AAO template was

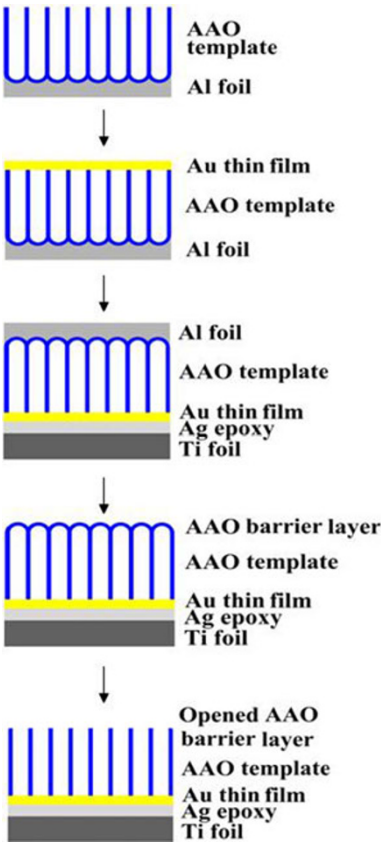

Fig. 1 Schematic diagram of the preparation stages of the AAO template for Pd nanowire electrodeposition

treated again in a 5 wt% phosphoric acid solution at 35°C for 20 min to remove the AAO barrier layer. Schematic diagram of the preparation stages of the AAO template for Pd nanowire electrodeposition was given in Fig. 1.

Electrodeposition was carried out in an aqueous solution containing $Pd(NH_3)_4Cl_2$ with NH_4Cl (pH value 7) at room temperature, using a three-electrode potentiostatic system(CHI 760C Electrochemical Workstation) with a saturated calomel electrode as a reference electrode and a graphite as a counter electrode. Pd was deposited using a potential of −1 V with 7,200 s deposition time. Then, to obtain free-standing Pd nanowires, the AAO template was dissolved with a 5 wt% NaOH solution for 10 min and then carefully rinsed away with deionized water. X-ray diffraction (XRD, Cu K_α, $\lambda = 0.154$ nm), scanning electron microscopy and energy-dispersive X-ray (SEM; EDX, Jeol JSM 6335) were used to study crystalline structures and morphologies of the fabricated Pd nanowires.

Results and discussion

The morphologies of the fabricated AAO template and Pd nanowire arrays were studied by SEM. Figure 2 shows

SEM images of the fabricated AAO template after the second anodization process. The detailed fabrication of AAO template with two-step anodization was given previously [25, 26]. The thickness and pore size of the AAO template can be controlled by changing the concentration of electrolytes, the time of anodic oxidation, time of pore widening and other conditions. Figure 2a shows top view of the AAO template, Fig. 2b shows a cross-sectional view of the AAO template and Fig. 2c shows a high magnification cross-sectional view of the AAO template. As clearly observed in Fig. 2, fabricated hexagonally straight AAO nanotubes were approximately 55 nm in diameter and 10 μm in length. The nanotubes exhibit almost perfect two-dimensional arrays with a hexagonal pattern. It shows that the formed nanotubes can be comparatively homogeneous without distorting the structures, resulting in them being highly oriented in one direction with a high aspect ratio of approximately 182. From these results, fabricated AAO nanotube density is approximately 2.59×10^{14} cm^{-2}. The nanotube density (ρ) is calculated as $2/\sqrt{3}\ D_{int}^{2} \times 10^{14}$ cm^{-2}, where D_{int} is the interpore distance.

As is seen in Fig. 3a, after dipping of the AAO template in $HgCl_2$ solution, all of metallic Al was removed according to following cementation reaction (1).

$$3HgCl_2 + 2Al \rightarrow 2AlCl_3 + 3Hg \quad (1)$$

The reaction products were cleaned from the remaining AAO template by rinsing with water. Hexagonal AAO barrier layers of all the AAO nanotubes were observed on the surface (Fig. 3a). The AAO barrier layers prevent the direct electrical contact between the AAO nanotubes and the Ti substrate, so that it is impossible to fill the nanotubes with Pd by electrodeposition. For electrodeposition of Pd in AAO template to be possible, the AAO barrier layers were opened to a bottom electrode. To remove the barrier layer, AAO template was treated with 5 wt% phosphoric acid solutions at 35°C for ca. 20 min. The SEM image of the obtained structure is given in Fig. 3b, which shows the surface of the AAO template with opened AAO barrier layer. Thus, the structure is ready for Pd electrodeposition.

Nucleation and growth kinetics in the initial stages of Pd deposition on Au electrode in AAO template were studied using the current transient technique. For electrodeposition of Pd, although the acidic $PdCl_2 \cdot 2HCl$ or $K_2PdCl_4 \cdot H_2SO_4$ electrolytes, the alkaline $Pd(NH_3)_4Cl_2$ or $Pd(NH_3)_2(NO_2)_2$ (P-salt type) electrolytes could be used, we worked with $Pd(NH_3)_4Cl_2 + NH_4Cl$ electrolyte as it is more chemically stable than the others. The mechanism of Pd electrodeposition on Au electrode depends strongly on the Pd–Au

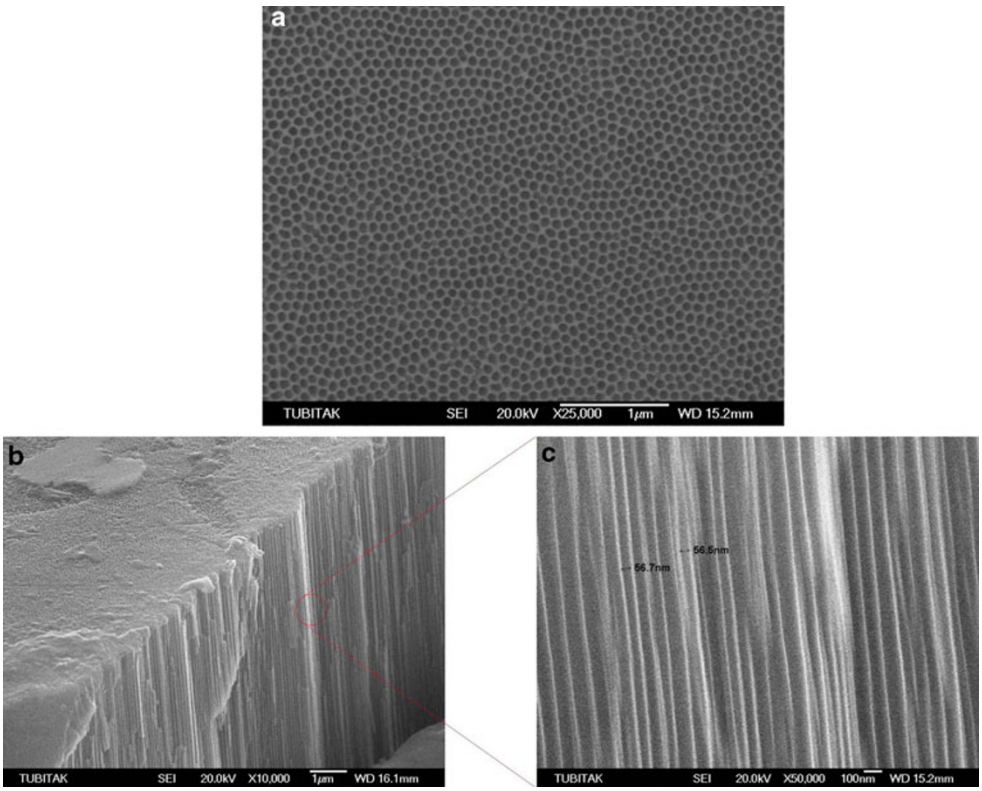

Fig. 2 SEM images of the fabricated AAO template. **a** Top view. **b** Cross-sectional view. **c** High-magnification cross-sectional view

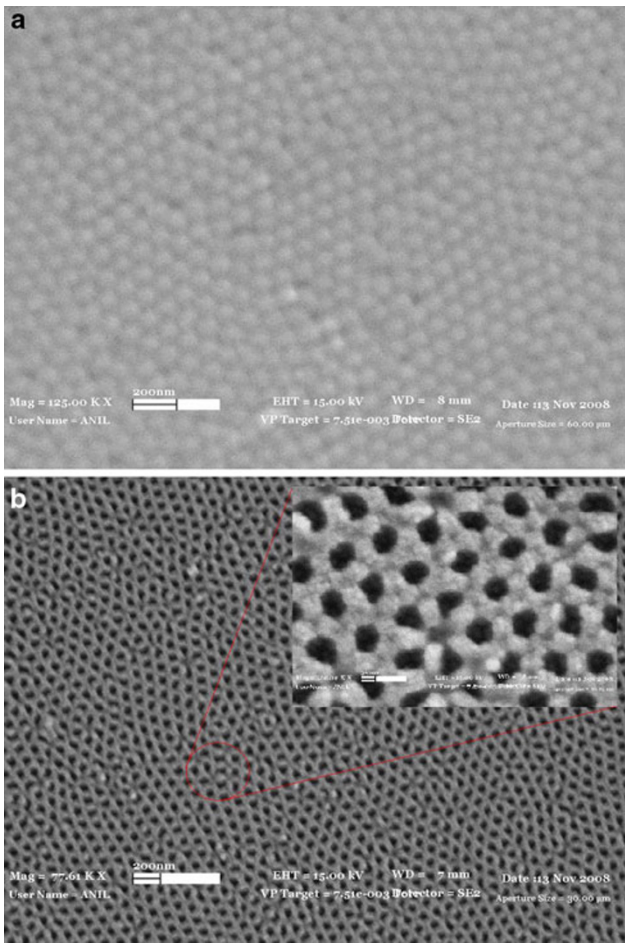

Fig. 3 SEM images of the AAO template. **a** Before removing the alumina barrier layer. **b** After removing of the alumina barrier layer

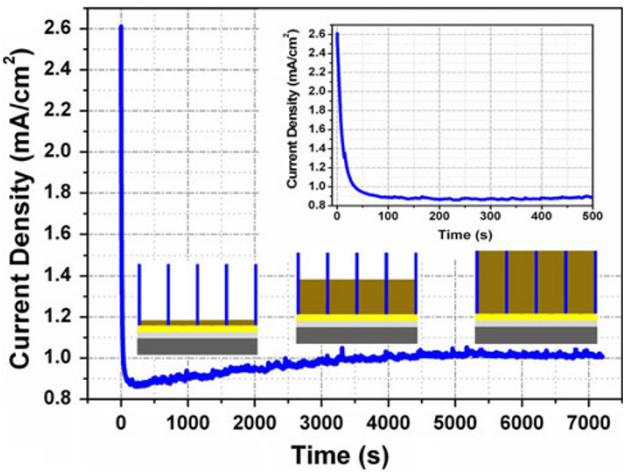

Fig. 4 The current transient during the electrodeposition of the Pd in the AAO template

interaction. The kinetics and the mechanism of Pd electrodeposition and the involved phase formation phenomena can also be influenced significantly by electronic properties of the Au substrate. Figure 4 shows the typical current transient for deposition of Pd.

As shown in Fig. 4, the electrodeposition of Pd nanowires is not a steady state process, and according to the Pd–Au interaction, the current–time transient shows a sharp drop in the initial current density due to the charging of the double layer, which was followed by a nonlinear increase in the current density with electrodeposition time. Such double-layer charging was also observed during electrodeposition of various metals [27–31]. But, on the contrary of previous studies, electrodeposition kinetic of Pd on Au electrode in AAO template, decreasing and then beginning to increase the current density, occurred in a very long time. Prior to the initiation of electrodeposition, palladium chloride forms $[PdCl_4]^{2-}$, palladium tetrachloro square-planar complex, with NH_4Cl dissolved in electrolyte as in the following reaction:

$$PdCl_2 + 2NH_4Cl^- \rightarrow [PdCl_4]^{2-} + 2NH_3 + 2H^+ \quad (2)$$

The reaction starts after formation and charging of the double layer of hydronium ions ($H^+ + H_2O = H_3O^+$) and $[PdCl_4]^{2-}$ ions on the Au electrode at the bottom of the AAO nanotubes. During the charging period, the current density decreases sharply with time. The $[PdCl_4]^{2-}$ ions are reduced by accepting electrons from the electrode through hydrogen-bonded (H_3O^+) ions. The Pd^{+2} solution used for the electrodeposition was 0.0085 M, and when the Pd^{+2} solution filled a nanotube of the AAO template that has 5.94×10^6 nm^3 volume, the number of the Pd^{+2} ions was approximately 30,258 in the mentioned AAO nanotube. To form a first atomic Pd^0 layer on the Au film at the bottom of the AAO nanotube, the process required approximately 120,878 Pd^{+2} ions. Therefore, the required process was diffusion controlled, and double layers at the AAO nanotubes of the template could form very slowly for this electrodeposition process (the initial stage of current density is given in top right of Fig. 4). After forming the double layers, current density starts to increase continuously with nonlinear characteristics.

The schematic view of growing of Pd in AAO template is given in Fig. 5. The discharging of Pd^0 to the Au electrode from the $[PdCl_4]^{2-}$ solution can be expressed as follows:

$$[PdCl_4]^{2-} + 2e^- \rightarrow Pd^0 + 4Cl^- \quad (3)$$

Discharging of Pd atoms forms the nuclei on the Au electrodes at the bottom of the AAO nanotubes. Pd atoms were continuously deposited on the Au electrode during the electrodeposition. As the Au electrode is negative in charge, the hydronium ion was attracted toward the electrode, forming a positive layer on the deposited palladium particles followed by a negative layer of $[PdCl_4]^{2-}$.

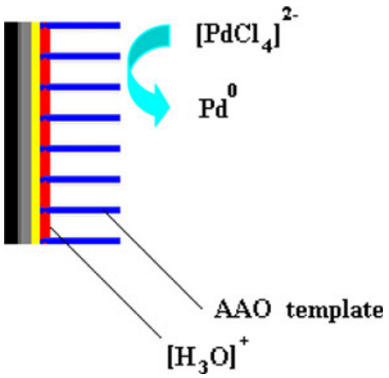

Fig. 5 The mechanism of Pd nucleation in AAO template

For understanding the growing mechanism of Pd nanowires, the log (current density)−log (time$^{1/2}$) transients need to be drawn (Fig. 6). It is clearly seen from Fig. 6 that current density in logarithmic scale is slowly decreased for a period and then decreased sharply to a minimum. After a steady state in this minimum for a period, the current density in logarithmic scale is increased. The increased part of log (current density)−log (time$^{1/2}$) graph is shown in the right top of the figure. The slope of the log (current density)−log (time$^{1/2}$) transient is approximately 0.13 A·cm^{-2}·s$^{-1/2}$, which indicates that the electrodeposition kinetic follows a parabolic relationship. This situation indicates an electrodeposition process of *spontaneous nucleation* and subsequent three-dimensional growth of formed nuclei. Therefore, the experimentally found out value of the number of the Pd nuclei density (N) can be calculated by using the following relation:

$$N = \frac{\rho^{1/2}}{{}_zF\pi(2Dc)^{3/2}M^{1/2}}k_P \quad (4)$$

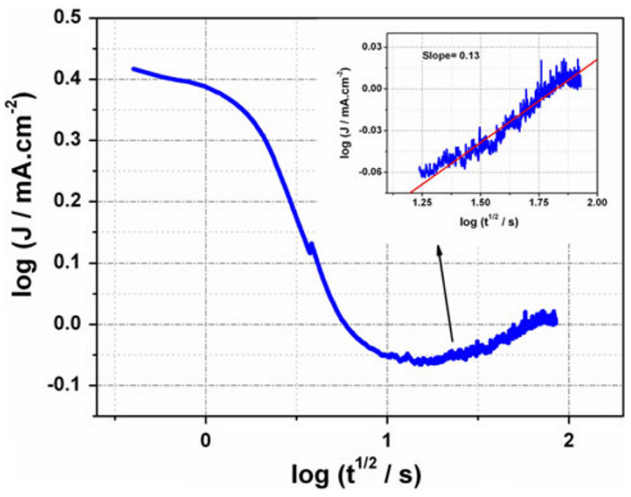

Fig. 6 Log (J)−log (t$^{1/2}$) graph for Pd electrodeposition in AAO template. The increasing part of Log (J)−log (t$^{1/2}$) graph is in the right top of the figure

Here, the value of the parabolic rate constant (k_P) was obtained from the slope of current density–$t^{1/2}$ transient. The electrodeposition current (I) usually obeys the following growth relation: where D is the diffusion coefficient, c is the concentration of metallic ions in the solution, zF is the effective molar charge of the electrodepositing species and t is time. M and ρ are the molecular weight and density of the metallic species deposited, respectively. In order to calculate Pd nuclei density, the values of described parameters are used as follows; $z = 2$, $F = 96{,}500$ Coulomb·mol^{-1}, $D = 6.70 \times 10^{-6}$ cm^2·s^{-1}, $M = 106.42$ g·mol^{-1}, $c = 2.087 \times 10^{-6}$ mol·cm^{-3}, and $\rho = 12.023$ g·cm^{-3}. Thus, for our nanodeposition, Pd nuclei density (N) is calculated as 3.55×10^8cm^{-2}. This value is approximately 1.116×10^5 cm^{-2} for electrodeposition of Pd on the highly oriented pyrolitic graphite (HOPG) [30]. The values of the N estimated for electrodeposition of Pd on HOPG in experimental conditions other than the present situation have been reported to be 5.8×10^9 and 3.6×10^8 cm^{-2} [31, 32]. The differences in the values are due to applied

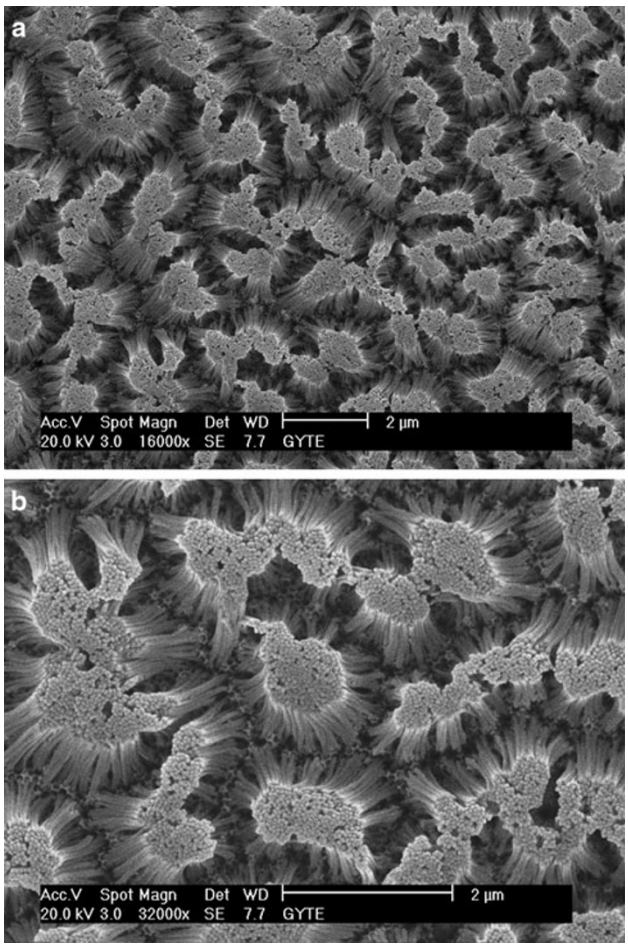

Fig. 7 **a** SEM image of Pd nanowires after removing the AAO template. **b** High-magnification SEM image of Pd nanowires

potential, concentration of the Pd ions in electrodeposition solutions and pH of the electrodeposition solutions.

Figure 7 shows the SEM images of Pd nanowires after dissolving the AAO template. It can be clearly observed from Fig. 7 that the Pd nanowires are highly ordered with uniform diameters approximately of 50 nm and lengths approximately 2.5 μm. The Pd nanowires are uniform and standing vertically to the electrode surface in a relatively large area, even though there are a few regions where the nanowires are absent. Therefore, the density of nanowires is almost close to the nanotube density of the fabricated AAO template. The Pd nanowires were not uniformly parallel to one another because of AAO-dissolving process in NaOH solution.

Figure 8a and b show a XRD spectrum and EDX spectra of the fabricated Pd nanowires, respectively. Fig. 8a confirms that the Pd nanowires possessed a face-centered cubic (fcc) structure and were well crystallized. The strong diffraction peaks at the Bragg angles of $2\theta = 40.20°$, 46.78° and 68.10° correspond to the (1 1 1), (2 0 0) and (2 2 0) reflection lines ,respectively, of the fcc phase of palladium.

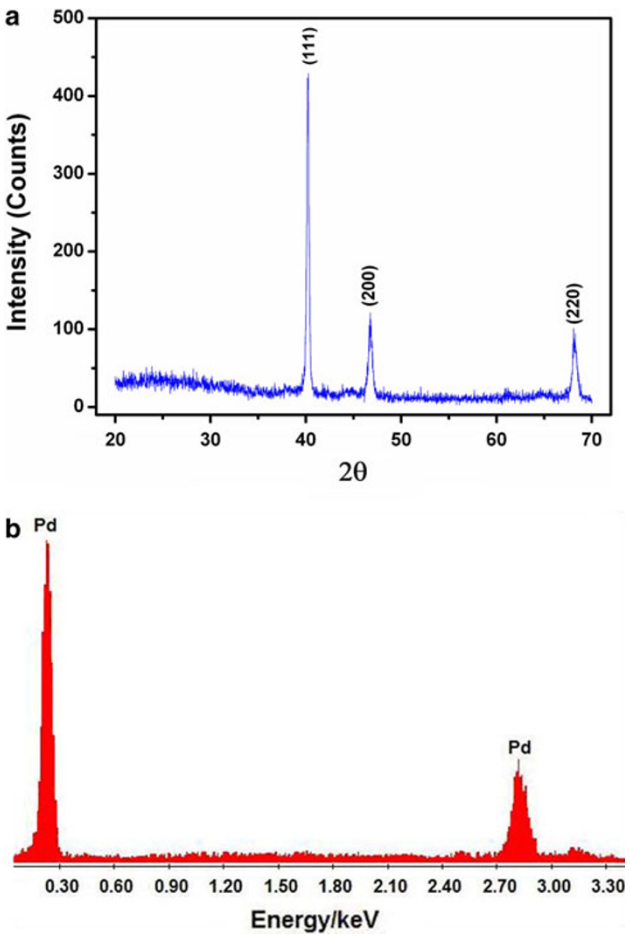

Fig. 8 **a** XRD spectrum from the surface of the Pd nanowires. **b** EDX spectra from the surface of the Pd nanowires

The sharp (1 1 1) peak is good evidence of palladium nanowires with high crystallinity compared to the results of Kartopu et al. [19]. Furthermore, the EDX spectrum (Fig. 8b) shows strong Pd signals from the fabricated Pd nanowires and confirms the electrodeposition of pure and high-crystalline Pd nanowires using dilute neutral electrolyte as electrodeposition medium.

Conclusions

Obtained vertically aligned Pd nanowires were approximately 50 nm in diameters and 2.5 μm in lengths with aspect ratio of 46. For determination of optimum growing rate, consequently high grade of nanowire crystallinity, the initial stages of the electrodeposition of Pd nanowires on Au were studied using potentiostat. Nucleation rate and the number of atoms in the critical nucleus are determined from the analysis of current transients. The fabricated Pd nanowires are well arranged (Fig. 7), have high crystallinity (Fig. 8) and also have less dislocations than fabricated known Pd nanowires due to slower nucleation rate. We believe that understanding the nucleation and growth mechanism in the electrodeposition process of Pd nanowires gives rise to fabricate higher purity, higher crystallinity, and lower dislocated Pd nanowires, suitable for potential nanotechnological applications especially in sensors.

Acknowledgments This study was supported by the Scientific and Technological Research Council of Turkey under the project title "Investigation and development of nanotechnologic hydrogen sensors" and Project No. 106T546.

Open Access This article is distributed under the terms of the Creative Commons Attribution Noncommercial License which permits any noncommercial use, distribution, and reproduction in any medium, provided the original author(s) and source are credited.

References

1. A. Huczko, Appl. Phys. A **70**, 365 (2000)
2. L. Vayssieres, Int. J Nanotechn. **1**, 1 (2004)
3. M.S. Dresselhaus, P. Avouris, in *Carbon Nanotubes: Synthesis, Structure, Properties and Application*, ed. by M.S. Dresselhaus, G. Dresselhaus, P.H. Avouris (Springer, Germany, 2000)
4. G. Zheng, W. Lu, S. Jin, C. Lieber, Adv. Mater. **16**, 1890 (2004)
5. E.S. Snow, F.K. Perkins, E.J. Houser, S.C. Badescu, T.L. Reinecke, Science **307**, 1942 (2005)
6. M. Tian, J. Wang, Q. Zhang, N. Kumar, T.E. Mallouk, M.H.W. Chan, Nano Lett. **9**, 3196 (2009)
7. J. Wang, C. Shi, M. Tian, Q. Zhang, N. Kumar, J.K. Jain, T.E. Mallouk, M.H.W. Chan, Phys. Rev. Lett. **102**, 247003 (2009)
8. A.P. Li, F. Müller, A. Birner, K. Nielsch, U. Gösele, Adv. Mater. **11**, 483 (1999)
9. H. Masuda, K. Fukuda, Science **268**, 1466 (1995)

10. O. Jessensky, F. Müller, U. Gösele, Appl. Phys. Lett. **72**, 1173 (1998)
11. A.L. Prieto, M.M. González, J. Keyani, R. Gronsk, T. Sands, A.M. Stacy, J Mater. Pro. Techn. **125**, 2388 (2003)
12. R.L. Zong, J. Zhou, Q. Li, B. Du, B. Li, M. Fu, X.W. Qi, L.T. Li, J Phys. Chem. **108**, 16713 (2004)
13. H.H. Wang, C.Y. Liu, S.B. Wu, N.W. Liu, C.Y. Peng, T.H. Chan, C.F.J. Hsu, K. Wang, Y.L. Wang, Adv. Mater. **18**, 491 (2006)
14. D.P. Smith, *Hydrogen in metals* (The University of Chicago Press, Chicago, 1948)
15. F.A. Lewis, *Palladium hydrogen system* (Academic Press, London/New York, 1967)
16. F. Favier, E.C. Walter, M.P. Zach, T. Benter, R.M. Penner, Science **293**, 2227 (2001)
17. K. Kim, M. Kim, S.M. Cho, Mater. Chem. Phys. **96**, 278 (2006)
18. K.T. Kim, S.J. Sim, S.M. Cho, The IEEE Sens. J **6**, 509 (2006)
19. G. Kartopu, S. Habouti, M. Es-Souni, Mater. Chem. Phys. **107**, 226 (2008)
20. F. Cheng, H. Wang, Z. Sun, M. Ning, Z. Cai, M. Zhang, Electrochem. Commun. **10**, 798 (2008)
21. S. Cherevko, N. Kulyk, J. Fu, C.H. Chung, Sens. Act. B **136**, 388 (2009)
22. E. Budevski, G. Staikov, W.J. Lorenz, *Electrochemical phase formation and growth an introduction to the initial stages of metal deposition* (VCH, Weinheim, 1996)
23. R. Krumm, B. Guel, C. Schmitz, G. Staikov, Electrochim. Acta **45**, 3255 (2000)
24. G. Oskam, J.G. Long, A. Natarajan, P.C. Searson, J Phys. D: Appl. Phys. **31**, 1927 (1998)
25. N. Taşaltın, S. Öztürk, N. Kılınç, H. Yüzer, Z.Z. Öztürk, Appl. Phys. A **95**, 781 (2009)
26. N. Taşaltın, S. Öztürk, N. Kılınç, H. Yüzer, Z.Z. Öztürk, J Optoelect. Biomed. Mater. **1**, 79 (2009)
27. H. Martin, P. Carro, A.H. Creus, S. González, R.C. Salvarezza, A.J. Arvia, Langmuir **13**, 100 (1997)
28. J.V. Zoval, R.M. Stiger, P.R. Biernacki, R.M. Penner, J Phys. Chem. **100**, 837 (1996)
29. B. Scharifker, G. Hills, Electrochim. Acta **28**, 879 (1983)
30. D. Bera, S.C. Kuiry, S. Seal, J Phys. Chem. B **108**, 556 (2004)
31. Y. Gimeno, A.H. Creus, P. Carro, S. Gonzalez, R.C. Salvarezza, A.J. Arvia, J Phys. Chem. B **106**, 4232 (2002)
32. Y. Gimeno, A.H. Creus, S. Gonzalez, R.C. Salverezza, A.J. Arvia, Chem. Mater. **13**, 1857 (2001)